This is a preprint, the final version is subject to change, of the American Mineralogist (MSA)
Cite as Authors (Year) Title. American Mineralogist, in press.
DOI: https://doi.org/10.2138/am-2019-7033

1 **Revision 2**

2 Sound Velocity of Neon at High Pressures and Temperatures 3 by Brillouin Scattering

4 **WEI WEI[1], XINYANG LI[1], NINGYU SUN[1], SERGEY N. TKACHEV[3],**

5 **AND ZHU MAO[1,2,*]**

6 [1]Laboratory of Seismology and Physics of Earth's Interior, School of Earth and Space
7 Sciences, University of Science and Technology of China, Hefei, China

8 [2]CAS Center for Excellence in Comparative Planetology, China

9 [3]Center for Advanced Radiation Sources, University of Chicago, Chicago, IL, USA

10

11

12

13

14

15

16

17

18

19

*Corresponding author: zhumao@ustc.edu.cn

This is a preprint, the final version is subject to change, of the American Mineralogist (MSA)
Cite as Authors (Year) Title. American Mineralogist, in press.
DOI: https://doi.org/10.2138/am-2019-7033

ABSTRACT

In this study, we have determined the combined effect of pressure and temperature on the compressional-wave velocity (V_P) of Ne up to 53 GPa and 1100 K using Brillouin scattering in externally-heated diamond anvil cells. The phase transition from the supercritical fluid to solid phase was observed to cause a 10.5-11% jump in V_P, and the magnitude in the V_P contrast across the phase transition increases with temperature. In addition, we have observed an abnormal reduced increase rate of V_P with pressure in the supercritical Ne fluid at both 800 and 1100 K before the transition to the solid phase. V_P of the solid Ne exhibits a non-linear increase with pressure at all the investigated temperatures. Elevating temperature was noted to cause an apparent reduction in V_P, yet the reduction in V_P caused by increasing temperature dramatically decreases at higher pressures. At 20 GPa, increasing temperature by 100 K can lower the V_P of Ne by 2.4%. Yet elevating temperature by 100 K only can reduce the V_P by 0.4% at 50 GPa. We further compare V_P of Ne to that of other rare gases, including Ar, Kr, and Xe. At 300 K, V_P of Ne shows a stronger dependence on pressure than both Kr and Xe. Moreover, increasing temperature can produce a greater reduction in V_P of Ne than that of Ar below 50 GPa. Our measured V_P of Ne is also useful for understanding the velocity structure of giant planets, such as Jupiter.

Keywords: Ne, Sound velocity, High pressure and temperature, Brillouin scattering, Rare gases

1. Introduction

Earth's interior is at the extremely high pressure and temperature (P-T) conditions. The development of diamond anvil cells (DACs) combined with a variety of optical and synchrotron X-ray techniques enable us to investigate the physical and chemical properties of minerals at relevant P-T conditions of the Earth's deep interior (e.g., Bassett 1979, 2009, Jayaraman 1983, 1986; Polsky and Valkenburg 2006; Mao et al. 2016). In the DAC experiments, it is critical to maintain a quasi-hydrostatic condition at high pressures with the use of pressure medium to minimize the differential stress and ensure that the pressure inside the DACs is homogeneous (Piermarini et al. 1973; Angel et al. 2007; Takemura 2007b, 2007a; Klotz et al. 2009). Neon (Ne) is one of the most commonly used pressure media in the high-pressure studies (e.g. Jephcoat et al. 1986; Fei et al. 2007; Dewaele et al. 2008; Zhuravlev et al. 2010; Dorfman et al. 2012). It can maintain a better quasi-hydrostatic condition than soft solids (e.g. NaCl, KCl), alcohol mixture, and some rare gases (Ar, Xe, Kr) at high pressures (Meng et al. 1993; Miletich et al. 2000; Takemura 2007b; Klotz et al. 2009). Although both He and H_2 can maintain a better hydrostaticity than Ne at high pressures, diamonds with He or H_2 as the pressure

This is a preprint, the final version is subject to change, of the American Mineralogist (MSA)
Cite as Authors (Year) Title. American Mineralogist, in press.
DOI: https://doi.org/10.2138/am-2019-7033

media inside the DACs are easier to break and fail at high pressures (Takemura 2001, 2007a; Dewaele and Loubeyre 2007; Klotz et al. 2009). Ne is thus one of the most desirable pressure media in high-pressure studies. In addition, the deep interior of giant planets, such as Jupiter, is expected to contain a certain amount of Ne (Wilson and Militzer 2010). Based on the measurements from the Galileo probe, the concentration of Ne in the Jupiter's atmosphere is one order of magnitude lower than that of the protosolar, indicating that a certain amount of Ne may dissolve in the helium raindrops and fall into the planetary deep interior (Roulston and Stevenson 1995; Niemann et al. 1996; Wilson and Militzer 2010). Knowledge of the physical properties of Ne at high P-T conditions is also important for understanding the structure of giant planets.

At 300 K, the supercritical Ne fluid crystallizes in the face-centered-cubic (fcc) structure at 4.7 GPa (Finger et al. 1981; Vos et al. 1991). No phase transition was identified for Ne up to 236 GPa at 300 K (Hemley et al. 1989; Dewaele et al. 2008; Takemura et al. 2010). The melting temperature of Ne follows a linear increase with pressure up to 70 GPa and exhibits a much weak dependence on pressure (Vos et al. 1991; Solca et al. 1998; Datchi and Loubeyre 2000; Santamaría-Pérez et al. 2010). Between 20 and 40 GPa, the melting temperature of Ne is 700-1600 K lower than that of Ar, Kr, and Xe (Zha et al. 1986; Boehler et al. 2001; Ross et al. 2005; Santamaría-Pérez et al. 2010). In particular, the

This is a preprint, the final version is subject to change, of the American Mineralogist (MSA)
Cite as Authors (Year) Title. American Mineralogist, in press.
DOI: https://doi.org/10.2138/am-2019-7033

77 elasticity of Ne is important in understanding its bonding character and phase stability at
78 high P-T conditions. It was experimentally determined between 0.2 and 7 GPa at 300 K
79 using Brillouin spectroscopy (Shimizu et al. 2005). Theoretical studies extended the
80 investigated pressure up to 100 GPa at 0 K and reported a near-linear increase in the
81 single-crystal elasticity of Ne with pressure, although Gupta and Goyal (2009) suggested
82 that both C_{11} and C_{44} of solid Ne exhibit a slightly reduced increase rate with pressure
83 between 60 and 100 GPa at 0 K (Tsuchiya and Kawamura 2002; Shimizu et al. 2005;
84 Zarochentsev et al. 2006; Pechenik et al. 2008; Gupta and Goyal 2009). The sound
85 velocity of Ne was also determined below 300 K at 1 bar to 1 GPa (Batchelder et al. 1967;
86 Balzer et al. 1971; Kortbeek et al. 1988). At 1 bar, Ne crystallizes at 24.4 K, and both
87 compressional- (V_P) and shear-wave velocity follow a nonlinear decrease with
88 temperature from 0 K to ~24 K (Batchelder et al. 1967; Balzer et al. 1971). At a given
89 temperature between 98 and 298 K, V_P of Ne exhibits a non-linear increase with pressure
90 up to 0.8 GPa (Kortbeek et al. 1988). To date, we still lack experimental constraints on
91 the sound velocity of Ne at simultaneously high P-T conditions above 7 GPa and 300 K.
92
93 In this study, we have measured the sound velocity of polycrystalline Ne using Brillouin
94 scattering in externally-heated diamond anvil cells (EHDACs) at simultaneously high P-T
95 conditions up to 53 GPa and 1100 K. Our results provide crucial constraints on the

96 combined effect of pressure and temperature on the sound velocity of Ne. We further
97 compared the velocity of Ne with other heavier rare gases for understanding their
98 characters at high P-T conditions.
99

100 2. Experimental details

101 High P-T experiments were performed using the BX90 EHDACs with 300-μm culet
102 diamonds (Kantor et al. 2012). Two Pt foils, placed 80 μm away from the diamond culet
103 center and separated by 90^{o}, were used as the pressure calibrant (Fei et al., 2007). A ruby
104 sphere was also loaded into the EHDAC as the pressure indicator during Ne loading.
105 Temperature was determined by an R-type thermocouple which was placed ~500 μm
106 away from the culet edge. A ring-shaped alumina ceramic heater coiled by two
107 platinum-rhodium wires was attached on top of one diamond and used as the heat supply.
108 The heater was placed around the anvils to provide a steady and sustained
109 high-temperature environment. The temperature gradient in our EHDAC is within ±5 K.
110 Ne was pressurized at room temperature into the EHDACs using the gas loading system
111 at the GSECARS of the Advanced Photon Source (APS), Argonne National Laboratory
112 (ANL). The supercritical Ne fluid was captured in the sample chamber during remote
113 closing of the DAC. High P-T Brillouin scattering measurements were performed up to
114 53 GPa and 1100 K at 13-BMD, GSECARS of the APS, ANL. The sound velocity of Ne

This is a preprint, the final version is subject to change, of the American Mineralogist (MSA)
Cite as Authors (Year) Title. American Mineralogist, in press.
DOI: https://doi.org/10.2138/am-2019-7033

115 was measured at 300, 550, 800, and 1100 K at high pressures, respectively. Brillouin
116 spectra were collected in the forward scattering geometry with an external scattering
117 angle of 50° using a six-pass Sandercock tandem Fabry-Perot interferometer (Figure 1).
118 Acoustic velocities of Ne were calculated using the measured Brillouin frequency shift,
119 $\Delta\upsilon_B$, following equation:

120 $$V = \frac{\Delta\upsilon_B \lambda_0}{2\sin(\theta/2)},$$

121 where V is the acoustic velocity, λ_0 is the incident laser wavelength (532 nm), θ is
122 the external scattering angle. At selected P-T conditions, we rotated the sample by 120^o to
123 examine the potential anisotropy of our polycrystalline Ne. After each high P-T Brillouin
124 measurement, we have also collected the X-ray diffraction pattern of Pt to determine the
125 pressure (Fei et al. 2007). The sound velocity of Ne at 300 K was measured after the
126 temperature quench to minimize the deviatoric stress inside the EHDAC.
127

128 ## 3. Results and discussion

129 Figure 1 shows the typical Brillouin spectra of Ne at high P-T conditions. In most
130 collected Brillouin spectra, only V_P of the solid Ne was observed because the shear wave
131 was too weak to be detected by our Brillouin measurements or was shown as a tiny bump
132 which cannot yield reliable constraints on the shear-wave velocity. Here we have also
133 examined the anisotropy of our polycrystalline Ne by rotating the sample over 120^o at a

given P-T condition (Figure 2). Below 23 GPa, solid Ne inside the EHDACs maintained an excellent hydrostaticity at 550 K. Yet increasing pressure produced a weak anisotropy in the investigated solid Ne. The variation of V_P was noted to be within ±3.5% above 23 GPa at 550 K (Figure 2). Our high P-T measurements have shown that V_P of Ne followed a non-linear increase with pressure at a given temperature (Figure 3). Increasing temperature was noted to cause an apparent decrease in V_P, and the effect of temperature on V_P of Ne dramatically weakens at higher pressures (Figures 3 and 4). At 20 GPa, elevating temperature by 100 K leads to a 2.4% decrease in V_P, whereas it can only lower V_P by 0.4% at 50 GPa (Figure 4). Here we have also calculated the density of Ne using the thermal equations of state in Fei et al. (2007) and constructed the relationship of V_P with density up to 53 GPa and 1100 K. At 300 K, V_P of Ne increases linearly with density following the Birch's law (Birch 1961). Yet it exhibits a weak non-linear dependence on density at high temperatures. In addition, we have also observed a decrease in V_P with increasing temperature at a given density.

Although we lack experimental constraints on V_P of Ne below 9 GPa at 300 K, our measured V_P above 9 GPa follows the same trend with pressure as V_P in Shimizu et al. (2005) for solid Ne between 4.6 and 7 GPa (Figure 3). We further compared our obtained V_P with the theoretical predictions which were performed at 0 K (Figure 5) (Tsuchiya and

This is a preprint, the final version is subject to change, of the American Mineralogist (MSA)
Cite as Authors (Year) Title. American Mineralogist, in press.
DOI: https://doi.org/10.2138/am-2019-7033

153 Kawamura 2002; Zarochentsev et al. 2006; Pechenik et al. 2008; Gupta and Goyal 2009).
154 Although these theoretical calculations yield conflicting results on V_P of Ne at high
155 pressures and 0 K, they all predicted a non-linear increase in V_P which is similar to our
156 observation (Tsuchiya and Kawamura 2002; Zarochentsev et al. 2006; Pechenik et al.
157 2008; Gupta and Goyal 2009). It is interesting to note that the supercritical fluid to solid
158 phase transition in Ne at 300 K can cause a sudden increase by 10.5 % in V_P at 4.7 GPa
159 (Shimizu et al., 2005). Here we observed a discontinuous increase in V_P of Ne at both 800
160 K and 1100 K, which should be associated with the supercritical fluid to solid phase
161 transition (Figure 3). An abnormal reduced increasing rate of V_P was observed at 13 GPa
162 and 800 K before the supercritical Ne fluid transitioned into the solid phase, and a similar
163 abnormal reduced increase rate occurred around 24 GPa at 1100 K. Yet the unusual
164 reduced increase rate of V_P before the occurrence of the supercritical fluid-solid phase
165 transition may not be apparent at relatively low temperatures and thus was not observed
166 at 550 K in this study and at 300 K in the literature (Shimizu et al. 2005). Due to limited
167 experimental data points, here we can only provide an estimation on the velocity jump at
168 high temperatures. The supercritical fluid to solid phase transition at 800 K around 15
169 GPa is estimated to produce a 10% (± 1.5%) jump in V_P. At 1100 K, V_P of Ne exhibits a
170 much weaker dependence on pressure from 24 GPa, and the V_P contrast between the
171 supercritical fluid and solid phases is about 11% (± 3%) (Figure 3).

This is a preprint, the final version is subject to change, of the American Mineralogist (MSA)
Cite as Authors (Year) Title. American Mineralogist, in press.
DOI: https://doi.org/10.2138/am-2019-7033

172

173 Heavier rare gases such as Ar, Kr and Xe are also important pressure media in high
174 pressure experiments (e.g. Liebenberg 1979; Asaumi and Ruoff 1986; Jephcoat et al.
175 1986; Mao et al. 1986; Klotz et al. 2009). We further compare V_P of Ne with that of the
176 other rare gases mentioned above to understand the bonding characters of these simple
177 molecule solids at high pressures (Figure 6) (Grimsditch et al. 1986; Polian et al. 1989;
178 Kume et al. 1998; Shimizu et al. 2001; Sasaki et al. 2009; Chen et al. 2010; Marquardt et
179 al. 2013). Although previous experimental studies normally grew single-crystal rare gases
180 below 10 GPa and determined the single-crystal elasticity, these single crystals gradually
181 re-crystalized and turned into polycrystals at higher pressures (Chen et al., 2010;
182 Grimsditch et al. 1986; Polian et al. 1989; Kume et al. 1998; Marquardt et al., 2013;
183 Shimizu et al. 2001; Sasaki et al. 2009). As a result, sound velocities of the rare gases in
184 literature above 10 GPa were usually measured in various directions at a given pressure,
185 and the maximum and minimum measured values were used to describe the directional
186 dependence of the sound velocity (Grimsditch et al. 1986; Polian et al. 1989; Kume et al.
187 1998; Shimizu et al. 2001; Sasaki et al. 2009; Chen et al. 2010). Figure 6 shows the
188 measured maximum and minimum V_P of rare gases from the literature to compare them
189 with our results for solid Ne. It is worth noting that previous experimental studies yield
190 conflicting results on the maximum (minimum) V_P of Ar between 4 and 70 GPa at 300 K

This is a preprint, the final version is subject to change, of the American Mineralogist (MSA)
Cite as Authors (Year) Title. American Mineralogist, in press.
DOI: https://doi.org/10.2138/am-2019-7033

191 (Figure S1) (Grimsditch et al., 1986; Shimizu et al., 2001; Marquardt et al., 2013; Chen et
192 al., 2010). Here we showed the largest (lowest) value of the maximum (minimum) V_P of
193 Ar (Figure 6).
194
195 In contrast to Ar, Xe, and Kr, solid Ne remains in the fcc structure up to 236 GPa at 300
196 K (Hemley et al. 1989; Dewaele et al. 2008; Takemura et al. 2010). Yet both Kr and Xe
197 were observed to transform from the fcc structure to the hexagonal-closest-packed (hcp)
198 phase below 3 GPa, and the fcc and hcp phases could coexist up to 70-140 GPa (Cynn et
199 al. 2001; Errandonea et al. 2002, 2006; Rosa et al. 2018). Although Sasaki et al. (2009)
200 observed a splitting of V_P in the Brillouin measurements at 10 GPa which could be related
201 to the fcc to hcp phase transition, the measured sound velocity in other studies did not
202 exhibit any anomaly at 10 GPa (Polian et al. 1989; Kume et al. 1998). The reported value
203 in literature above 5-10 GPa for both Xe and Kr should thus be a combined velocity of
204 the fcc and hcp phases (Polian et al. 1989; Kume et al. 1998; Sasaki et al. 2009). Here we
205 have noted that V_P of Ne is much greater than that of Xe and Kr at high pressures and
206 exhibits a stronger dependence on pressure (Figure 6). Comparing the V_P of Ne to the
207 average of the maximum and minimum V_P of Kr and Xe has shown that, at 10 GPa, the
208 difference in V_P between Ne and Xe (Kr) is 26% (17%). At 30 GPa, the difference in V_P
209 between Ne and Xe (Kr) increases to 33% (23%).

This is a preprint, the final version is subject to change, of the American Mineralogist (MSA)
Cite as Authors (Year) Title. American Mineralogist, in press.
DOI: https://doi.org/10.2138/am-2019-7033

Due to the conflicting results of Ar in previous studies, it is hard to directly compare the V_P of Ne to Ar at high pressures and 300 K (Figure 6 and S1) (Grimsditch et al. 1986; Shimizu et al. 2001; Chen et al. 2010; Marquardt et al. 2013). For comparison, we choose the V_P data in Marquardt et al. (2013) which provided constraints on the V_P of Ar at simultaneously high P-T conditions. The hcp-Ar was reported to coexist with the fcc phase from 49.6 GPa at 300 K, but previous studies did not observe any notable discontinuity in the sound velocity across the phase transition up to 70 GPa (Shimizu et al. 2001; Errandonea et al. 2006; Marquardt et al. 2013). Like Ne, V_P of Ar increases smoothly with pressure at both 300 K and 700 K up to 70 GPa. Although V_P of Ne exhibits a stronger dependence on temperature, elevating temperature has a minor effect on the V_P of Ar. The temperature dependence of V_P for Ne dramatically decreases with increasing pressure (Figure 7). In contrast to Ne, the effect of temperature on the V_P of Ar reaches the maximum at 27 GPa and starts to weaken gradually with increasing pressure above 27 GPa (Figure 7). At 20 GPa, elevating temperature from 300 K to 700 K can cause a 9.6% reduction in the V_P of Ne but only lowers the V_P of Ar by 2.4% (Figure 7b). At 50 GPa, increasing temperature to 700 K can cause a similar reduction in the V_P of Ne to Ar. The effect of temperature on Kr and Xe at high pressures is unknown and needs further investigation.

229

230 ## 4. Implications

231 Compared to other giant planets in the solar system, Jupiter is best characterized due to
232 the measurements of the Galileo probe (Niemann et al. 1996; Seiff et al. 1996, 1998;
233 Little 1999). Based on the measurements of the Jupiter atmosphere from the Galileo
234 probe, a certain amount of Ne is expected to dissolve in the helium droplets (Roulston
235 and Stevenson 1995; Wilson and Militzer 2010). The predicted separation of hydrogen
236 and helium will cause Ne to concentrate in the mantle of Jupiter below the
237 hydrogen-helium immiscibility line (Roulston and Stevenson 1995; Wilson and Militzer
238 2010). Our measured V_P of Ne is useful for understanding the velocity structure of giant
239 planets, such as Jupiter. The phase diagram of Ne has shown that it should be present as
240 supercritical fluid in the mantle of Jupiter according to the speculated P-T conditions
241 (Saumon and Guillot 2004; Santamaría-Pérez et al. 2010; Nettelmann et al. 2012;
242 Militzer and Hubbard 2013). Here, our measurements have shown that V_P of the
243 supercritical Ne fluid exhibits a downward trend with increasing pressure above 800 K.
244 Increasing pressure has a weak effect on the V_P of the supercritical Ne fluid at 800 K and
245 1100 K, although there are only two data points for the supercritical Ne fluid at 1100 K. It
246 indicates that the variation in temperature has a stronger effect on the V_P of the
247 supercritical Ne fluid than pressure. The mantle temperature of Jupiter was predicted to

248 be between 6300 and 21000 K (Guillot 1999). Under such high temperature conditions,
249 V_P of the supercritical Ne fluid in the Jupiter's mantle will be much less than 5 km/s. Our
250 *in-situ* high P-T results together with phase boundary thus provide the fundamental
251 knowledge on velocity characters of Ne at high P-T conditions, which can help to reveal
252 new insights on the velocity structure of the Jupiter.
253
254 In summary, we have determined the V_P of Ne at simultaneously high P-T conditions
255 using Brillouin scattering up to 53 GPa and 1100 K. The solidification of Ne was
256 observed to cause a sudden increase in V_P. Furthermore, an abnormal reduced increase
257 rate of the V_P in the supercritical Ne fluid was observed at both 800 K and 1100 K before
258 the phase transition. Such abnormal reduced increase rate of the V_P did not appear below
259 550 K. At all the investigated temperatures, V_P of solid Ne follows a non-linear increase
260 with pressure, which is similar to other rare gases, such as Ar, Kr, Xe. Yet V_P of Ne
261 exhibits a stronger dependence on pressure than Xe and Kr. Elevating temperature at a
262 given pressure leads to a linear decrease in V_P. It is interesting to note that the effect of
263 temperature on V_P of solid Ne dramatically weakens at higher pressures. Increasing the
264 temperature by 100 K at 20 GPa can lower V_P of Ne by 2.4%, yet the reduction drops to
265 0.4% at 50 GPa. In addition, temperature has a stronger effect on V_P of Ne than that of Ar

266 below 50 GPa. Future studies are expected to provide constraints on the combined effect
267 of pressure and temperature on the sound velocity of other rare gases.

268

269 ## Acknowledgements

270 Z. Mao acknowledges supports from the National Science Foundation of China
271 (41874101, 41590621), and the Strategic Priority Research Program of the Chinese
272 Academy of Sciences (XDB18000000). This work was performed at GeoSoil-
273 EnviroCARS, Advanced Photon Source, Argonne National Laboratory, supported by the
274 National Science Foundation (EAR-1634415) and Department of Energy
275 (DE-FG02-94ER14466). Use of the COMPRES-GSECARS gas loading system was
276 supported by COM-PRES under NSF Cooperative Agreement EAR 1606856.

277

278 **REFERENCES**
279
280 Angel, R.J., Bujak, M., Zhao, J., Gatta, G.D., and Jacobsen, S.D. (2007) Effective
281 hydrostatic limits of pressure media for high-pressure crystallographic studies. Journal of
282 Applied Crystallography, 40, 26–32.
283 Asaumi, K., and Ruoff, A.L. (1986) Nature of the state of stress produced by xenon and
284 some alkali iodides when used as pressure media. Physical Review B, 33, 5633–5636.
285 Balzer, R., Kupperman, D.S., and Simmons, R.O. (1971) Velocities of sound in
286 polycrystalline neon. Physical Review B, 4, 3636–3639.
287 Bassett, W.A. (1979) Geophysical Applications of High Pressure Research. In
288 High-Pressure Science and Technology pp. 1033–1048.
289 Bassett, W.A. (2009) Diamond anvil cell, 50th birthday. High Pressure Research, 29,
290 163–186.
291 Batchelder, D.N., Losee, D.L., and Simmons, R.O. (1967) Measurements of lattice
292 constant, thermal expansion, and isothermal compressibility of neon single crystals.
293 Physical Review, 162, 767–775.
294 Birch, F. (1961) The velocity of compressional waves in rocks to 10 kilobars: 2. Journal
295 of Geophysical Research, 66, 2199–2224.
296 Boehler, R., Ross, M., Söderlind, P., and Boercker, D.B. (2001) High-pressure melting
297 curves of argon, krypton, and xenon: Deviation from corresponding states theory.
298 Physical Review Letters, 86, 5731–5734.
299 Chen, B., Gleason, A.E., Yan, J.Y., Koski, K.J., Clark, S., and Jeanloz, R. (2010)
300 Elasticity, strength, and refractive index of argon at high pressures. Physical Review B -
301 Condensed Matter and Materials Physics, 81, 1–5.
302 Cynn, H., Yoo, C.S., Baer, B., Iota-Herbei, V., McMahan, A.K., Nicol, M., and Carlson,
303 S. (2001) Martensitic fcc-to-hcp transformation observed in xenon at high pressure.
304 Physical Review Letters, 86, 4552–4555.
305 Datchi, F., and Loubeyre, P. (2000) Extended and accurate determination of the melting
306 curves of argon, helium, ice and hydrogen. Physical Review B - Condensed Matter and
307 Materials Physics, 61, 6535–6546.
308 Dewaele, A., and Loubeyre, P. (2007) Pressurizing conditions in
309 helium-pressure-transmitting medium. High Pressure Research, 27, 419–429.
310 Dewaele, A., Datchi, F., Loubeyre, P., and Mezouar, M. (2008) High pressure-high
311 temperature equations of state of neon and diamond. Physical Review B - Condensed
312 Matter and Materials Physics, 77, 1–9.
313 Dorfman, S.M., Prakapenka, V.B., Meng, Y., and Duffy, T.S. (2012) Intercomparison of
314 pressure standards (Au, Pt, Mo, MgO, NaCl and Ne) to 2.5 Mbar. Journal of Geophysical
315 Research: Solid Earth, 117, 1–15.
316 Errandonea, D., Schwager, B., Boehler, R., and Ross, M. (2002) Phase behavior of

317 krypton and xenon to 50 GPa. Physical Review B - Condensed Matter and Materials
318 Physics, 65, 1–6.
319 Errandonea, D., Boehler, R., Japel, S., Mezouar, M., and Benedetti, L.R. (2006)
320 Structural transformation of compressed solid Ar: An x-ray diffraction study to 114 GPa.
321 Physical Review B - Condensed Matter and Materials Physics, 73, 2–5.
322 Fei, Y., Ricolleau, A., Frank, M., Mibe, K., Shen, G., and Prakapenka, V. (2007) Toward
323 an internally consistent pressure scale. Proceedings of the National Academy of Sciences,
324 104, 9182–9186.
325 Finger, L.W., Hazen, R.M., Zou, G., Mao, H.K., and Bell, P.M. (1981) Structure and
326 compression of crystalline argon and neon at high pressure and room temperature.
327 Applied Physics Letters, 39, 892–894.
328 Grimsditch, M., Loubeyre, P., and Polian, A. (1986) Brillouin scattering and three-body
329 forces in argon at high pressures. Physical Review B, 33, 7192–7200.
330 Guillot, T. (1999) Interiors of giant planets inside and outside the solar system. Science,
331 286, 72–77.
332 Gupta, S., and Goyal, S.C. (2009) Seismic wave velocities of rare gas solids through
333 elastic properties in Earth's lower mantle. Science in China Series D: Earth Sciences, 52,
334 1599–1611.
335 Hemley, R.J., Zha, C.S., Jephcoat, A.P., Mao, H.K., Finger, L.W., and Cox, D.E. (1989)
336 X-ray diffraction and equation of state of solid neon to 110 GPa. Physical Review B, 39,
337 11820–11827.
338 Jayaraman, A. (1986) Ultrahigh pressures. Review of Scientific Instruments, 57, 1013–
339 1031.
340 Jephcoat, A.P., Mao, H.K., and Bell, P.M. (1986) Static compression of iron to 78 GPa
341 with rare gas solids as pressure-transmitting media. Journal of Geophysical Research, 91,
342 4677.
343 Kantor, I., Prakapenka, V., Kantor, A., Dera, P., Kurnosov, A., Sinogeikin, S.,
344 Dubrovinskaia, N., and Dubrovinsky, L. (2012) BX90: A new diamond anvil cell design
345 for X-ray diffraction and optical measurements. Review of Scientific Instruments, 83.
346 Klotz, S., Chervin, J.C., Munsch, P., and Le Marchand, G. (2009) Hydrostatic limits of
347 11 pressure transmitting media. Journal of Physics D: Applied Physics, 42, 075413.
348 Kortbeek, P.J., van de Ridder, J.J., Biswas, S.N., and Schouten, J.A. (1988) Measurement
349 of the compressibility and sound velocity of Neon up to 1 GPa. International Journal of
350 Thermophysics, 9, 425–438.
351 Kume, T., Daimon, M., Sasaki, S., and Shimizu, H. (1998) High-pressure elastic
352 properties of liquid and solid krypton to 8 GPa. Physical Review B - Condensed Matter
353 and Materials Physics, 57, 13347–13350.
354 Liebenberg, D.H. (1979) A new hydrostatic medium for diamond anvil cells to 300 kbar
355 pressure. Physics Letters A, 73, 74–76.

356 Little, B. (1999) Galileo Images of Lightning on Jupiter. Icarus, 142, 306–323.
357 Mao, H.K., Xu, J., and Bell, P.M. (1986) Calibration of the ruby pressure gauge to 800
358 kbar under quasi-hydrostatic conditions. Journal of Geophysical Research, 91, 4673.
359 Mao, H.K., Chen, B., Chen, J., Li, K., Lin, J.F., Yang, W., and Zheng, H. (2016) Recent
360 advances in high-pressure science and technology. Matter and Radiation at Extremes, 1,
361 59–75.
362 Marquardt, H., Speziale, S., Gleason, A., Sinogeikin, S., Kantor, I., and Prakapenka, V.B.
363 (2013) Brillouin scattering and x-ray diffraction of solid argon to 65 GPa and 700 K:
364 Shear strength of argon at HP/HT. Journal of Applied Physics, 114, 093517.
365 Meng, Y., Weidner, D.J., and Fei, Y. (1993) Deviatoric stress in a quasi-hydrostatic
366 diamond anvil cell: Effect on the volume-based pressure calibration. Geophysical
367 Research Letters, 20, 1147–1150.
368 Miletich, R., Allan, D.R., and Kuhs, W.F. (2000) High-Pressure Single-Crystal
369 Techniques. Reviews in Mineralogy and Geochemistry, 41, 445–519.
370 Militzer, B., and Hubbard, W.B. (2013) Ab initio equation of state for hydrogen-helium
371 mixtures with recalibration of the giant-planet mass-radius relation. Astrophysical Journal,
372 774, 148.
373 Nettelmann, N., Becker, A., Holst, B., and Redmer, R. (2012) Jupiter models with
374 improved ab initio hydrogen equation of state (H-REOS.2). Astrophysical Journal, 750.
375 Niemann, H.B., Atreya, S.K., Carignan, G.R., Donahue, T.M., Haberman, J.A., Harpold,
376 D.N., Hartle, R.E., Hunten, D.M., Kasprzak, W.T., Mahaffy, P.R., and others (1996) The
377 Galileo probe mass spectrometer: Composition of Jupiter's atmosphere. Science, 272,
378 846–849.
379 Pechenik, E., Kelson, I., and Makov, G. (2008) Many-body model of rare gases at high
380 pressures. Physical Review B - Condensed Matter and Materials Physics, 78, 1–15.
381 Piermarini, G.J., Block, S., and Barnett, J.D. (1973) Hydrostatic limits in liquids and
382 solids to 100 kbar. Journal of Applied Physics, 44, 5377–5382.
383 Polian, A. (1992) Brillouin scattering studies of rare gas solids. High Pressure Research,
384 9, 205–217.
385 Polian, A., Besson, J.M., Grimsditch, M., and Grosshans, W.A. (1989) Solid krypton:
386 Equation of state and elastic properties. Physical Review B, 39, 1332–1336.
387 Polsky, C.H., and Valkenburg, E. Van (2006) The Diamond Anvil Cell. Handbook of
388 Vibrational Spectroscopy, 1352–1360.
389 Rosa, A.D., Garbarino, G., Briggs, R., Svitlyk, V., Morard, G., Bouhifd, M.A., Jacobs, J.,
390 Irifune, T., Mathon, O., and Pascarelli, S. (2018) Effect of the fcc-hcp martensitic
391 transition on the equation of state of solid krypton up to 140 GPa. Physical Review B, 97,
392 094115.
393 Ross, M., Boehler, R., and Soderlind, P. (2005) Xenon melting curve to 80 GPa and 5p-d
394 Hybridization. Physical Review Letters, 95, 5–8.

Santamaría-Pérez, D., Mukherjee, G.D., Schwager, B., and Boehler, R. (2010) High-pressure melting curve of helium and neon: Deviations from corresponding states theory. Physical Review B - Condensed Matter and Materials Physics, 81, 1–5.

Sasaki, S., Wada, N., Kume, T., and Shimizu, H. (2009) High-pressure Brillouin study of the elastic properties of rare-gas solid xenon at pressures up to 45 GPa. Journal of Raman Spectroscopy, 40, 121–127.

Saumon, D., and Guillot, T. (2004) Shock Compression of Deuterium and the Interiors of Jupiter and Saturn. The Astrophysical Journal, 609, 1170–1180.

Seiff, A., Kirk, D.B., Knight, T.C.D., Mihalov, J.D., Blanchard, R.C., Young, R.E., Schubert, G., von Zahn, U., Lehmacher, G., Milos, F.S., and others (1996) Structure of the Atmosphere of Jupiter: Galileo Probe Measurements. Science, 272, 844–845.

Seiff, A., Kirk, D.B., Knight, T.C.D., Young, R.E., Mihalov, J.D., Young, L.A., Milos, F.S., Schubert, G., Blanchard, R.C., and Atkinson, D. (1998) Thermal structure of Jupiter's atmosphere near the edge of a 5-μm hot spot in the north equatorial belt. Journal of Geophysical Research: Planets, 103, 22857–22889.

Shimizu, H., Tashiro, H., Kume, T., and Sasaki, S. (2001) High-pressure elastic properties of solid argon to 70 GPa. Physical Review Letters, 86, 4568–4571.

Shimizu, H., Imaeda, H., Kume, T., and Sasaki, S. (2005) High-pressure elastic properties of liquid and solid neon to 7 GPa. Physical Review B - Condensed Matter and Materials Physics, 71, 2–6.

Solca, J., Dyson, A.J., Steinebrunner, G., Kirchner, B., and Huber, H. (1998) Melting curves for neon calculated from pure theory. The Journal of Chemical Physics, 108, 4107–4111.

Takemura, K. (2001) Evaluation of the hydrostaticity of a helium-pressure medium with powder x-ray diffraction techniques. Journal of Applied Physics, 89, 662–668.

——— (2007a) Hydrostatic Experiments up to Ultrahigh Pressures. Journal of the Physical Society of Japan, 76, 202–205.

——— (2007b) Pressure scales and hydrostaticity. High Pressure Research, 27, 465–472.

Takemura, K., Watanuki, T., Ohwada, K., MacHida, A., Ohmura, A., and Aoki, K. (2010) Powder x-ray diffraction study of Ne up to 240 GPa. Journal of Physics: Conference Series, 215.

Tsuchiya, T., and Kawamura, K. (2002) First-principles study of systematics of high-pressure elasticity in rare gas solids , Ne , Ar , Kr , and Xe First-principles study of systematics of high-pressure elasticity in rare gas solids , Ne , Ar , Kr , and Xe, 5859.

Vos, W.L., Schouten, J.A., Young, D.A., and Ross, M. (1991) The melting curve of neon at high pressure. The Journal of Chemical Physics, 94, 3835–3838.

Wilson, H.F., and Militzer, B. (2010) Sequestration of noble gases in giant planet interiors. Physical Review Letters, 104, 1–4.

Zarochentsev, E. V., Varyukhin, V.N., Troitskaya, E.P., Chabanenko, V. V., and

Horbenko, E.E. (2006) Interatomic potential and elastic constants of rare-gas crystals under pressure. Physica Status Solidi (B) Basic Research, 243, 2672–2686.

Zha, C.S., Boehler, R., Young, D.A., and Ross, M. (1986) The argon melting curve to very high pressures. The Journal of Chemical Physics, 85, 1034–1036.

Zhuravlev, K.K., Jackson, J.M., Wolf, A.S., Wicks, J.K., Yan, J., and Clark, S.M. (2010) Isothermal compression behavior of (Mg,Fe)O using neon as a pressure medium. Physics and Chemistry of Minerals, 37, 465–474.

This is a preprint, the final version is subject to change, of the American Mineralogist (MSA)
Cite as Authors (Year) Title. American Mineralogist, in press.
DOI: https://doi.org/10.2138/am-2019-7033

442 Table 1. Measured V_P of Ne at high P-T

P (GPa)	T (K)	V_P (km/s)	State
9.5(1)	300	4.72(3)	Solid
9.6(1)	300	4.56(3)	Solid
10.9(2)	300	4.96(3)	Solid
11.5(2)	300	5.11(4)	Solid
14.2(2)	300	5.57(4)	Solid
21.2(4)	300	6.38(4)	Solid
23.4(4)	300	6.61(5)	Solid
27.3(4)	300	6.99(5)	Solid
3.5(1)	550	2.28(3)	Supercritical Fluid
4.0(1)	550	2.45(3)	Supercritical Fluid
7.4(2)	550	3.51(3)	Supercritical Fluid
11.1(2)	550	4.57(4)	Solid
11.9(2)	550	4.68(4)	Solid
12.2(2)	550	4.73(4)	Solid
13.7(2)	550	5.05(5)	Solid
14.0(2)	550	5.15(5)	Solid
15.0(3)	550	5.25(5)	Solid
16.1(2)	550	5.36(5)	Solid
16.6(2)	550	5.35(9)	Solid
18.0(2)	550	5.67(5)	Solid
18.4(1)	550	5.74(5)	Solid
20.7(2)	550	6.06(5)	Solid
22.7(4)	550	6.21(5)	Solid
24.8(4)	550	6.45(6)	Solid
27.0(6)	550	6.65(6)	Solid
31.7(3)	550	7.02(6)	Solid
35.3(5)	550	7.35(6)	Solid
40.0(1)	550	7.57(6)	Solid
49.6(5)	550	7.99(7)	Solid
3.8(1)	800	2.0(1)	Supercritical Fluid
9.2(2)	800	3.47(4)	Supercritical Fluid
9.8(2)	800	3.62(5)	Supercritical Fluid
12.9(2)	800	4.07(5)	Supercritical Fluid
18.2(3)	800	5.23(6)	Solid
23.3(3)	800	6.1(2)	Solid
26.7(3)	800	6.5(1)	Solid
33.5(2)	800	6.97(7)	Solid
38.4(4)	800	7.36(7)	Solid
19.6(2)	1100	4.8(1)	Supercritical Fluid
22.5(3)	1100	5.0(1)	Supercritical Fluid
27.9(2)	1100	6.1(1)	Solid
43.0(4)	1100	7.5(1)	Solid
43.9(4)	1100	7.6(1)	Solid
52.9(5)	1100	8.0(1)	Solid

This is a preprint, the final version is subject to change, of the American Mineralogist (MSA)
Cite as Authors (Year) Title. American Mineralogist, in press.
DOI: https://doi.org/10.2138/am-2019-7033

443 # Figure Caption

444 Figure 1. Representative Brillouin spectra of Ne at high P-T conditions. (**a**) at 35.3 GPa
445 and 550 K; (**b**) at 26.7 GPa and 800 K; (**c**) at 22.5 GPa and 1100 K. Black lines: collected
446 raw data; red lines: fitting results for the longitudinal modes (V_P); blue lines: fitting
447 results for the transverse modes (V_S).

448

449 Figure 2. Measured V_P of solid Ne at varying orientations. All the data points were
450 collected at 550 K. Blue: 8.6 GPa; green: 22.6 GPa; yellow: 31.7 GPa; lines: average
451 value of measured V_P.

452

453 Figure 3. V_P of Ne at high P-T conditions. (**a**) V_P of Ne as a function of pressure. The
454 insert figure shows the phase diagram of Ne. Solid lines: shown for readers to follow the
455 trend with increasing pressure; dashed grey line: phase boundary between the
456 supercritical fluid and solid Ne; solid line in the insert figure: melting curve of Ne
457 determined in this study; dashed line in the insert figure: melting curve of Ne from
458 previous studies (Vos et al. 1991; Santamaría-Pérez et al. 2010); (**b**) V_P of Ne as a
459 function of density. Open symbols: supercritical Ne fluid; solid symbols: solid Ne; circles:
460 this study; square: Shimizu et al. (2005); blue: 300 K; green: 550 K; orange: 800 K; red:
461 1100 K. Error bars are smaller than symbols when not shown.

462 Figure 4. Effect of temperature on V_P of solid Ne at a given pressure. (**a**) V_P of Ne at high
463 P-T conditions; (**b**) Variation of V_P at high pressures using V_P at 300 K as the reference.
464 Blue: 20 GPa; green: 30 GPa; orange: 40 GPa; red: 50 GPa. The standard deviations of
465 the calculated velocity are shown as $\pm 1\sigma$ at the bottom right corner of the figure.
466
467 Figure 5. Comparing V_P of Ne at high pressures and 300 K between this study and
468 literature results. Blue: experimental results at 300 K; black: theoretical predictions at 0 K
469 (Zarochentsev et al. 2006; Pechenik et al. 2008; Gupta and Goyal 2009); circles: this
470 study; squares: Shimizu et al. (2005); dashed line: Zarochentsev et al. (2006); short
471 dashed line: Pechenik et al. (2008); dashed dotted line: Gupta and Goyal (2009).
472
473 Figure 6. Comparing V_P of Ne to other rare gases at high pressure and 300 K. Red: Ne
474 (this study); blue: Ar (Grimsditch et al. 1986; Shimizu et al. 2001; Chen et al. 2010;
475 Marquardt et al. 2013); green: Kr (Polian et al. 1989; Kume et al. 1998); orange: Xe
476 (Sasaki et al. 2009); circles: experimental data of Ne in this study; squares: experimental
477 data of Ne from Shimizu et al. (2005); dashed line: V_P of Xe and Kr calculated using the
478 corresponding single-crystal elastic moduli (Kume et al. 1998; Sasaki et al. 2009); shaded
479 area : the upper and lower bounds of V_P for polycrystalline Ar, Xe, and Kr in literature

This is a preprint, the final version is subject to change, of the American Mineralogist (MSA)
Cite as Authors (Year) Title. American Mineralogist, in press.
DOI: https://doi.org/10.2138/am-2019-7033

480 (Grimsditch et al. 1986; Polian 1992; Shimizu et al. 2001; Sasaki et al. 2009; Chen et al.
481 2010; Marquardt et al. 2013).

482

483 Figure 7. Effect of temperature on V_P of Ne and Ar at high pressures. (**a**) V_P at high P-T
484 conditions. Red: Ne (this study); blue: Ar (Marquardt et al. 2013); solid lines: 300 K;
485 dashed lines: 700 K; (**b**) Variation of V_P at high pressures using V_P at 300 K as the
486 reference. Red: Ne; blue: Ar (Marquardt et al. 2013). The standard deviations of the
487 calculated velocity are shown as $\pm 1\sigma$ at the bottom left corner of the figure.

488

489

This is a preprint, the final version is subject to change, of the American Mineralogist (MSA)
Cite as Authors (Year) Title. American Mineralogist, in press.
DOI: https://doi.org/10.2138/am-2019-7033

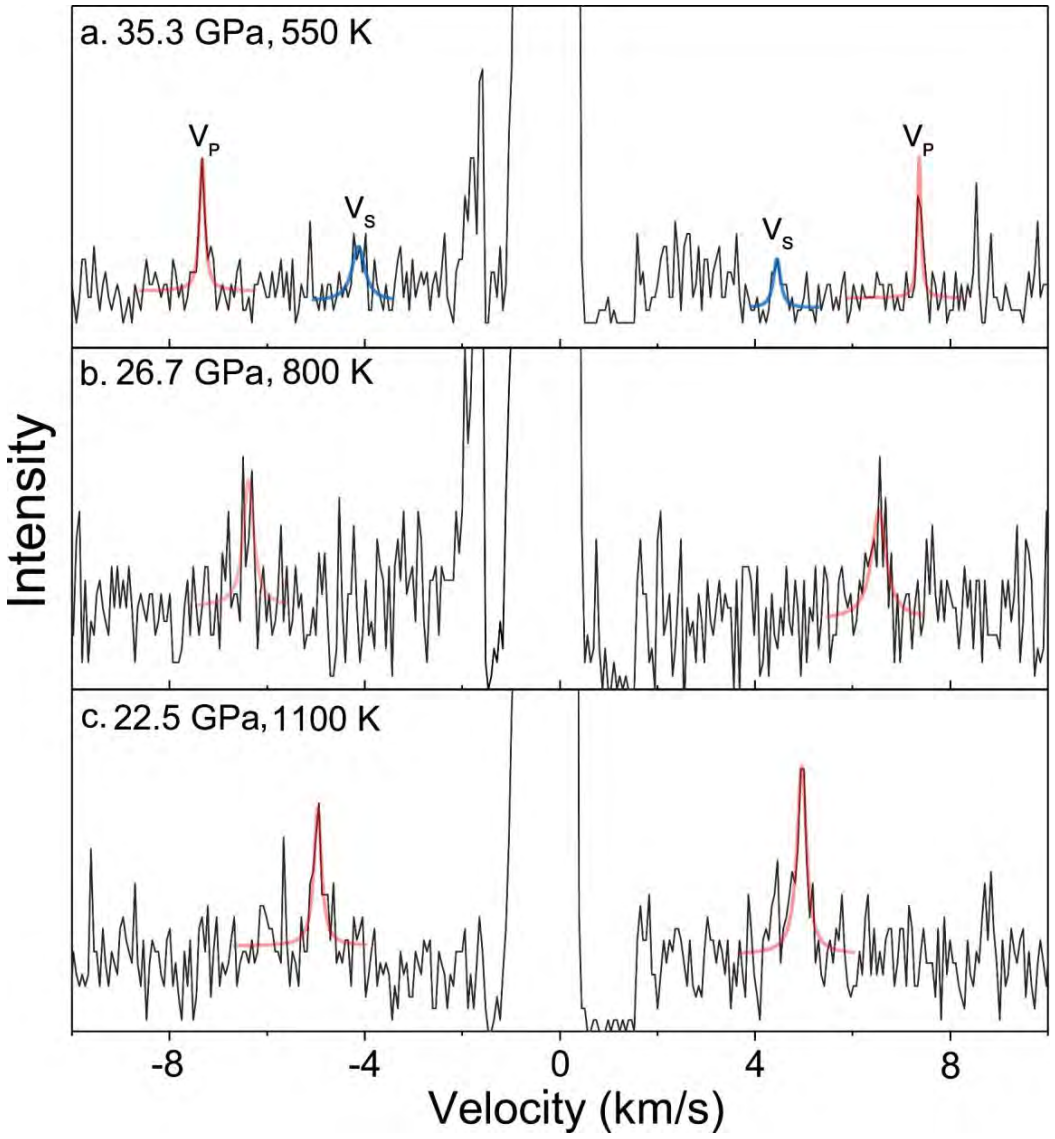

Figure 1

This is a preprint, the final version is subject to change, of the American Mineralogist (MSA)
Cite as Authors (Year) Title. American Mineralogist, in press.
DOI: https://doi.org/10.2138/am-2019-7033

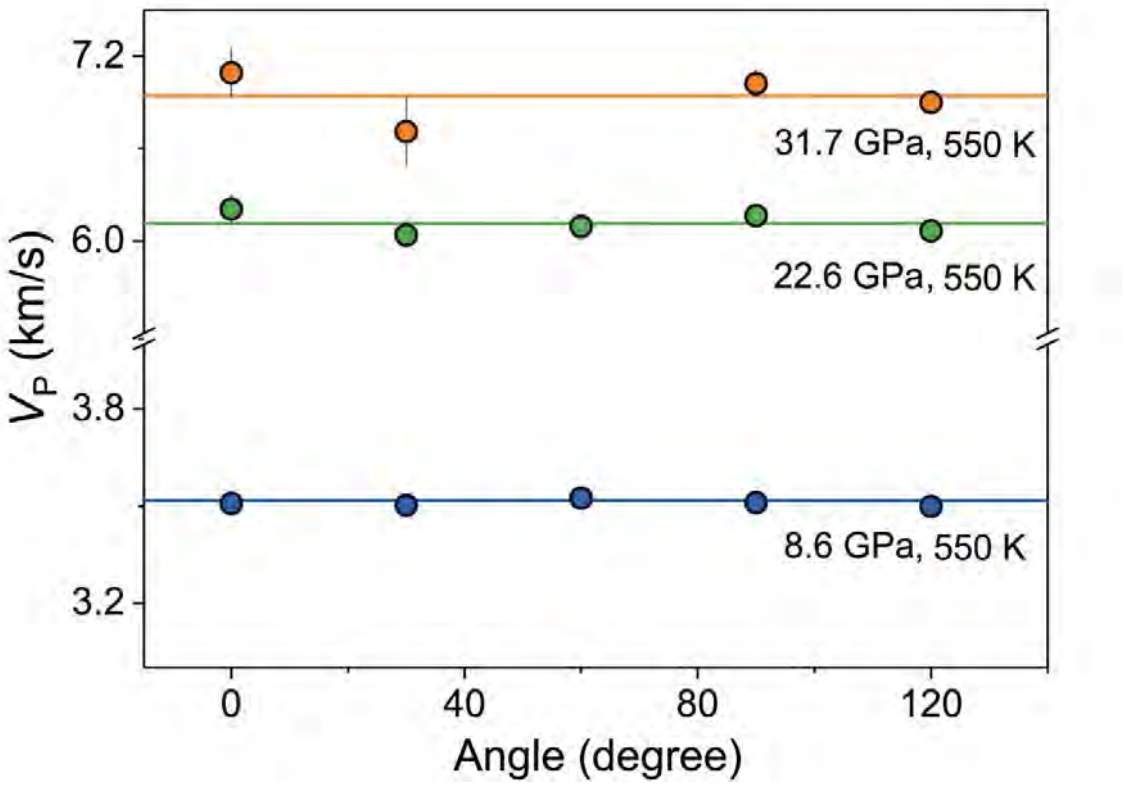

Figure 2

This is a preprint, the final version is subject to change, of the American Mineralogist (MSA)
Cite as Authors (Year) Title. American Mineralogist, in press.
DOI: https://doi.org/10.2138/am-2019-7033

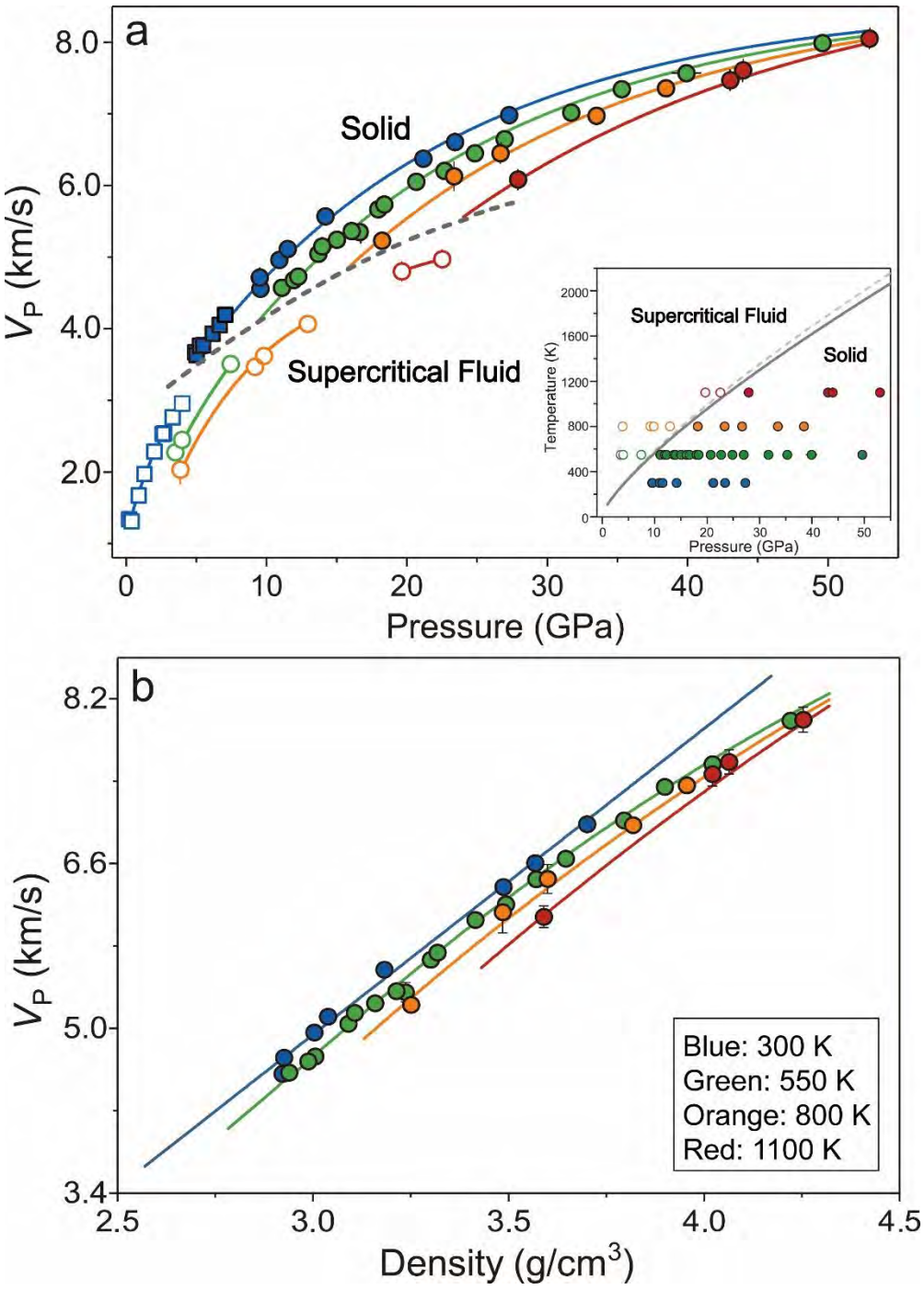

Figure 3

This is a preprint, the final version is subject to change, of the American Mineralogist (MSA)
Cite as Authors (Year) Title. American Mineralogist, in press.
DOI: https://doi.org/10.2138/am-2019-7033

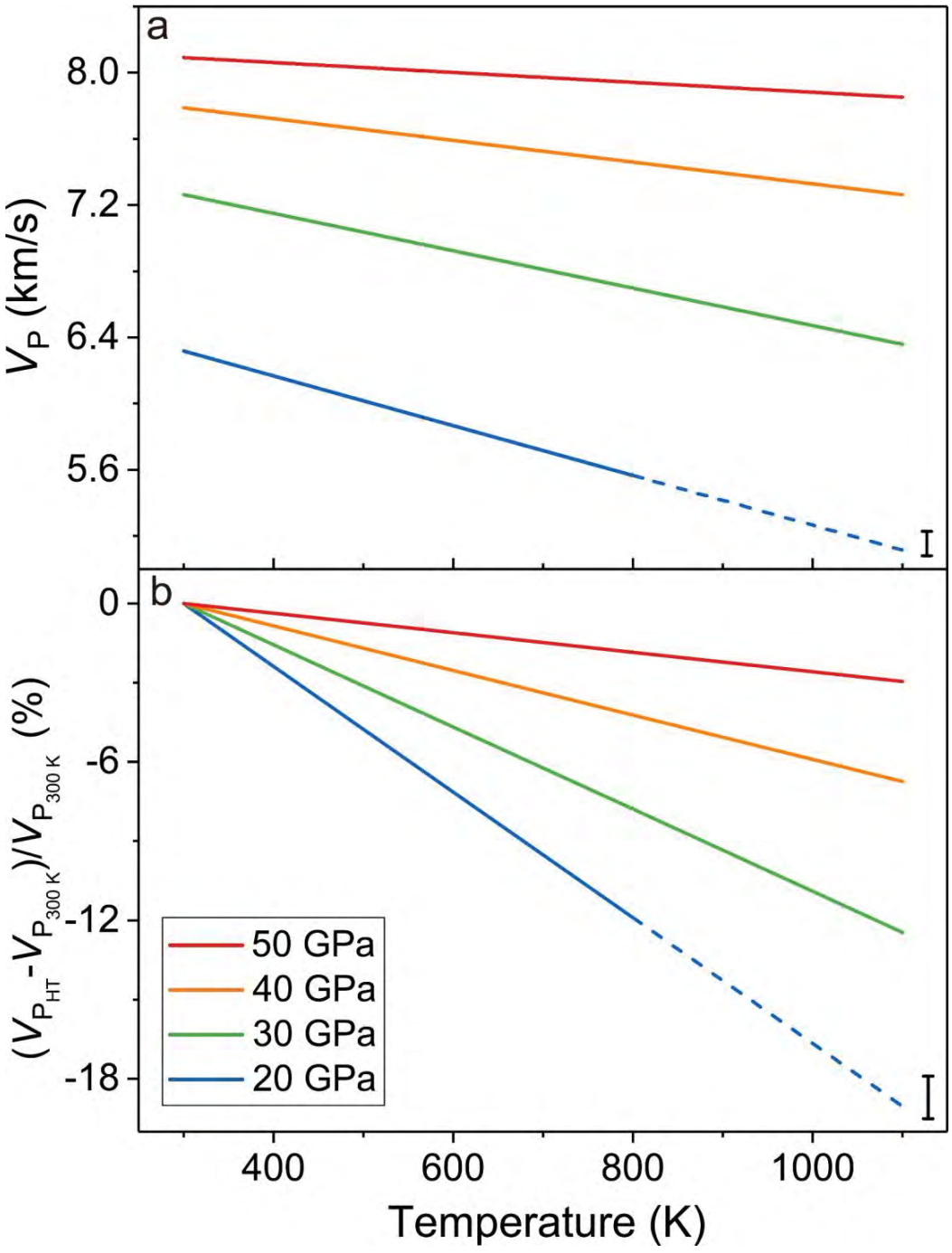

Figure 4

This is a preprint, the final version is subject to change, of the American Mineralogist (MSA)
Cite as Authors (Year) Title. American Mineralogist, in press.
DOI: https://doi.org/10.2138/am-2019-7033

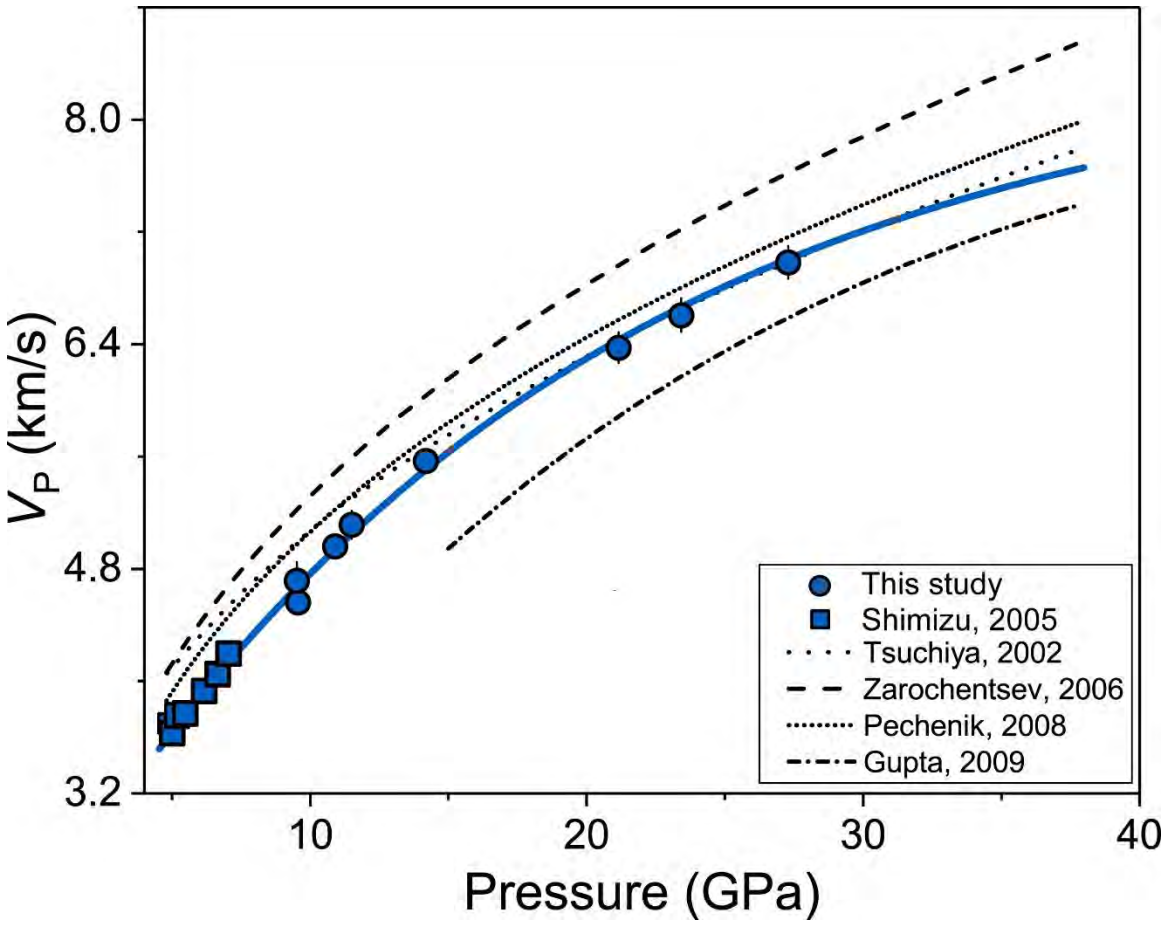

Figure 5

This is a preprint, the final version is subject to change, of the American Mineralogist (MSA)
Cite as Authors (Year) Title. American Mineralogist, in press.
DOI: https://doi.org/10.2138/am-2019-7033

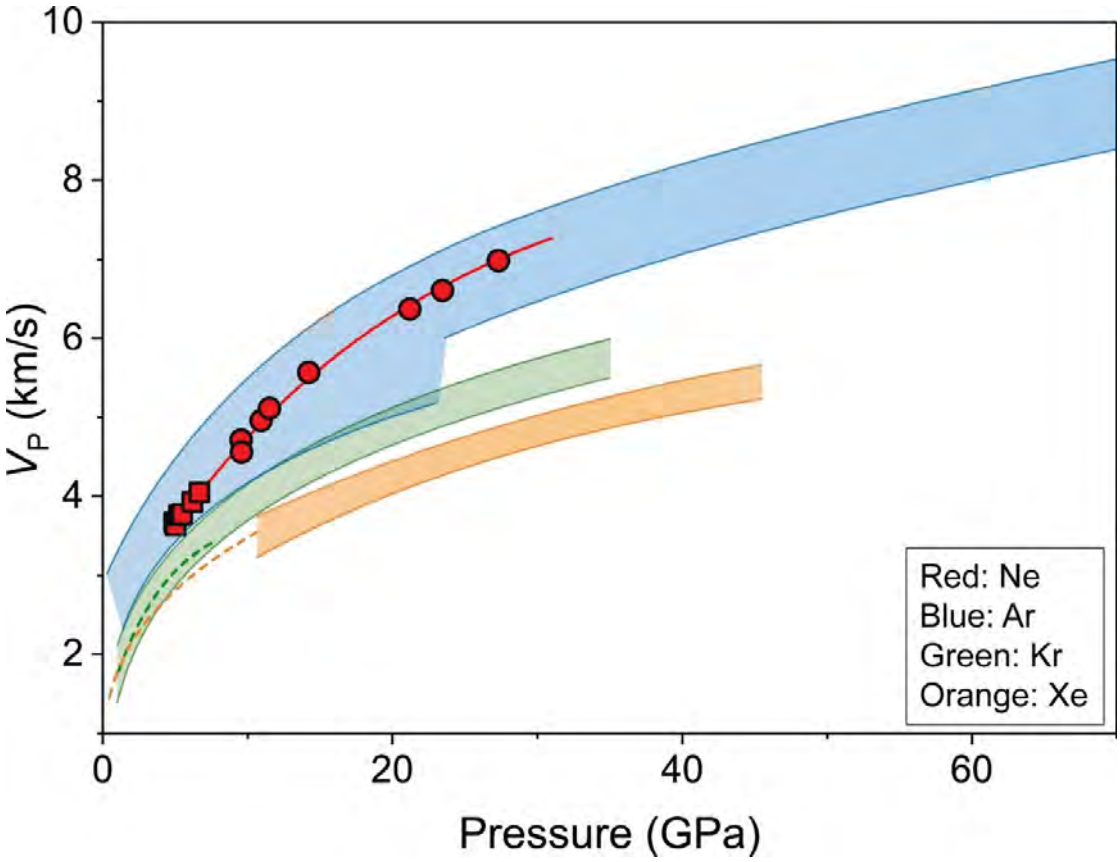

Figure 6

This is a preprint, the final version is subject to change, of the American Mineralogist (MSA)
Cite as Authors (Year) Title. American Mineralogist, in press.
DOI: https://doi.org/10.2138/am-2019-7033

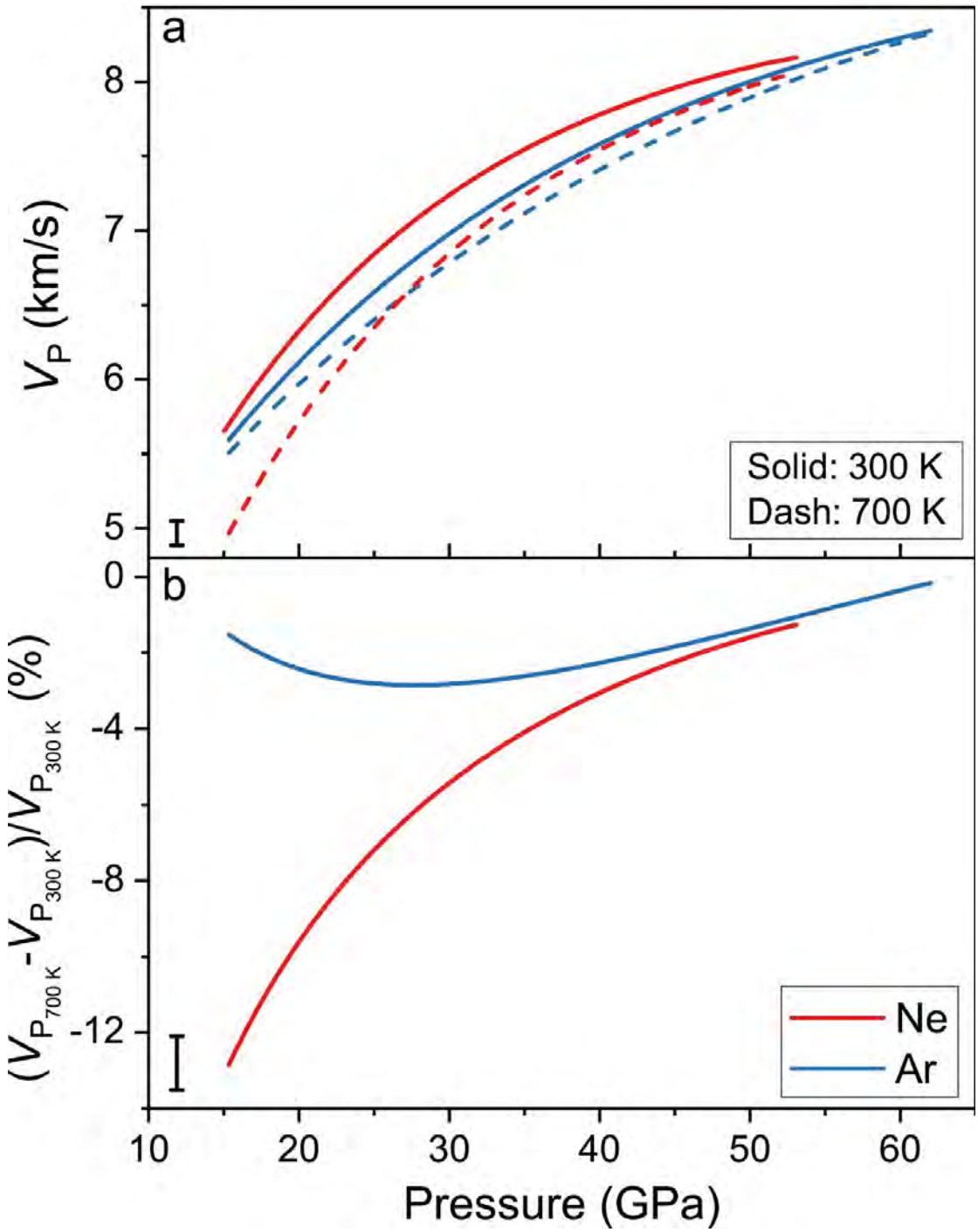

Figure 7